Peptide-Mediated Growth and Dispersion of Au Nanoparticles in Water *via* Sequence Engineering

Michelle A. Nguyen,[1,#] Zak E. Hughes,[2,#†] Yang Liu,[3] Yue Li,[3] Mark T. Swihart,[3] Marc R. Knecht,[1,] and Tiffany R. Walsh[2,]**

[1]Department of Chemistry, University of Miami, 1301 Memorial Drive, Coral Gables, Florida 33146, United States

[2]Institute for Frontier Materials, Deakin University, Geelong, Victoria 3216, Australia

[3]Department of Chemical and Biological Engineering, University at Buffalo (SUNY), Buffalo, New York 14260, United States

(#: These authors contributed equally)

† Present Address: School of Chemistry and Biosciences, University of Bradford, Bradford, BD7 1DP, UK

RECEIVED DATE (to be automatically inserted after your manuscript is accepted if required according to the journal that you are submitting your paper to)

*To whom correspondence should be addressed: MRK: Phone: (305) 284-9351, email: knecht@miami.edu; TRW: Phone: +61 (35) 227-3116, email: tiffany.walsh@deakin.edu.au

Abstract

The use of peptides to nucleate, grow, and stabilize nanoparticles in aqueous media via non-covalent interactions offers new possibilities for creating functional, water-dispersed inorganic/organic hybrid materials, particularly for Au nanoparticles. Numerous previous studies have identified peptide sequences that both possess a strong binding affinity for Au surfaces and are capable of supporting nanoparticle growth in water. However, recent studies have shown that not all such peptide sequences can produce stable dispersions of these nanoparticles. Here, via integrated experiments and molecular modeling, we provide new insights into the many factors that influence Au nanoparticle growth and stabilization in aqueous media. We define colloidal stability by the absence of visible precipitation after at least 24 hours post-synthesis. We use binding affinity measurements, nanoparticle synthesis, characterization and stabilization assays, and molecular modeling, to investigate a set of sequences based on two known peptides with strong affinity for Au. This set of biomolecules is designed to probe specific sequence and context effects using both point mutations and global reorganization of the peptides. Our data confirm, for a broader range of sequences, that Au nanoparticle/peptide binding affinity alone is not predictive of peptide-mediated colloidal stability. By comparing nanoparticle stabilization assay outcomes with molecular simulations, we establish a correlation between the colloidal stability of the Au nanoparticles and the degree of conformational diversity in the surface-adsorbed peptides. Our findings suggest future routes to engineer peptide sequences for bio-based growth and dispersion of functional nanoparticles in aqueous media.

Keywords: peptides, mutations, nanoparticles, binding affinity, stabilization.

Introduction

Bio-inspired peptide-mediated strategies are an effective approach to nucleate, grow, stabilize, activate, and organize inorganic nanoparticles in aqueous media.[1] Despite these successes, broader applicability of such strategies is limited by a lack of fundamental understanding of how to manipulate the surface-adsorbed structure, and consequently the binding strength and concomitant properties, of materials-binding peptides. Previous studies[2-4] have demonstrated that a peptide sequence with strong materials-binding affinity does not necessarily also serve as an effective agent for stabilizing a dispersion of peptide-capped nanoparticles. The reasons for this disconnect are currently unknown. This drives the need to identify the features of peptide sequences that can promote strong materials-binding affinity, effective nanoparticle stabilization capability, or both.

Alteration of peptide sequences (*e.g. via* point mutations or by sequence scrambling) has been used in prior investigations of peptide binding affinity and nanoparticle stabilization.[3, 5] However, detailed molecular-level structural data that would enable clear conceptual links between a given peptide sequence, its bound conformation(s) on a surface, and the peptide's ability to cap and stabilize inorganic nanoparticles are still far from comprehensive, and remain much needed for advancing our understanding of this problem. For example, a point mutation can eliminate surface binding at that particular point in the sequence, but it might also lead to large-scale conformational changes throughout the rest of the peptide when it is adsorbed onto the particle surface. This lack of a predictable response to mutations severely hinders clear interpretation of experiments that seek to identify which residues are the most critical for mediating surface binding to nanomaterials.

As a critical first step to addressing this challenging problem, here we aim to progress the systematic construction of a structure/property knowledge-base for peptide-stabilized

nanomaterials. To do this, we build on two concepts that were introduced in prior work. The first is the concept of anchor residues.[6] We define anchor residues to be those residues that are known to interact strongly with gold (from predictions of amino acid binding strengths[7]), namely Trp, Tyr, Arg, Met, and to some extent Phe and His, and that support a strong degree of residue-metal surface contact of 80% or greater. Our definition makes a distinction between residues that make strong contact with the surface due to specific interactions, as opposed to residues that can coincidentally be found close to the surface but are not considered strong binders, such as Ala (based on amino acid binding data[7]). A second concept used throughout the present study is conformational susceptibility, which we introduced in earlier studies[3] to interpret the structural outcomes of point mutations in materials-binding peptides. Briefly, a sequence is conformationally susceptible if point mutations of an anchor residue to Ala resulted in a distinct difference in the conformational ensemble of the peptide. We consider a conformationally recalcitrant peptide to be a sequence that features minimal structural change following such point mutations.

In this work we have quantified and elucidated how the mutations of two different parent peptide sequences with very different conformational susceptibilities can influence both the non-covalent binding affinity at aqueous Au interfaces, and the ability of these biomolecules to nucleate, grow, and stabilize Au nanoparticles (NPs) in aqueous media. Specifically, we provide an in depth analysis and characterization of the Au-binding behavior of mutants of two well-known Au-binding sequences: A3 (AYSSGAPPMPPF) and AuBP1 (WAGAKRLVLRRE). Our mutation studies provide new insights into the sequence characteristics that control peptide-materials binding affinity, and can explain how and why particular mutants of these sequences can stabilize Au NPs in solution. Following previous work,[3] we considered five sequence

variations each for A3 and AuBP1, as summarized in Table 1. For the two parent peptides, we replaced each known anchor residue (identified from our previous work[6]) with alanine (sequences A3-1 to A3-3, and AuBP1-1 to AuBP1-3). We also considered a randomized version of each peptide sequence (A3-4 and AuBP1-4) and a variation of the peptide sequence in which all anchor residues were grouped together at the N-terminus (A3-5 and AuBP1-5). Including the original parent biomolecules, this gives a total of twelve unique peptide sequences. Through a combination of quartz crystal microbalance (QCM) measurements, NP synthesis and characterization, and advanced molecular dynamics (MD) simulations, we have quantified and evaluated how each of these twelve sequences adsorbs to Au surfaces and the ability of each of these peptides to support the nucleation, growth, and stabilization of Au NPs in aqueous media. Our results provide key insights into the effects of local sequence context (*i.e.* the impact of the neighboring residues surrounding anchor residues) on the binding of peptides to their target inorganic surface, providing a pathway toward the *de novo* design of new sequences with enhanced binding affinity and NP stabilization capability.

Materials and Methods

Chemicals. Ammonium hydroxide (20%) and hydrogen peroxide (30%) were purchased from BDH Chemicals. $HAuCl_4$ and $NaBH_4$ were obtained from Sigma-Aldrich. The peptides used were acquired from Genscript at >90% purity. All chemicals employed in this study were used as received without further purification. Milli-Q water (18 MΩ·cm) was used for all experiments.

QCM Binding Experiments. All QCM measurements, including those for dissipation energy, were conducted using a Q-Sense E4 instrument (Biolin Scientific) following

established methods.[6, 8] Standard polycrystalline Au crystal sensors were cleaned according to manufacturer protocols before use. Briefly, the Au QCM sensors were subjected to UV-ozone exposure, followed by immersion in a 5:1:1 (v/v/v) water/ammonium hydroxide/hydrogen peroxide solution and an additional UV/ozone treatment. An aqueous peptide solution at a concentration of 2.5 to 15 μg/mL was flowed over the sensor surface at a rate of 150 μL/min. The frequency change and dissipation energy were recorded for 30 min to ensure saturation. The frequency change is directly related, *via* the Sauerbrey equation, to the mass of peptide adsorbed, from which rate parameters for binding can be determined.[6, 9] All QCM experiments were performed at 22.5 °C, and the pH of the peptide solutions ranged from 4.1 – 6.0 depending on the sequence. Peptide solutions were prepared by dissolving the peptide in deionized water at the appropriate concentration.

Au nanoparticle synthesis. Peptide-capped Au NPs were prepared according to synthetic methods established by Li *et al*.[10] In a typical experiment, 500 μL of an aqueous 1.0 mM peptide solution was added to 4.460 mL of water in a vial. Next, 10 μL of an aqueous 100 mM $HAuCl_4$ solution was added. The solution was briefly agitated and allowed to stand for 10 min before adding 30 μL of a freshly prepared aqueous 100 mM $NaBH_4$ solution. A $NaBH_4$:Au ratio of 3 was used for all syntheses. The solution was briefly agitated, and the reaction was allowed to proceed undisturbed at room temperature for 1.0 h to ensure complete reduction.

Nanoparticle characterization. Once fabricated, the NPs were optically characterized using a Shimadzu 3600 UV-vis-NIR spectrophotometer with a 1 cm path length quartz cuvette. The size and shape of the Au NPs were characterized using a JEOL JEM-2010

TEM operating at a working voltage of 200 kV. Samples were prepared for imaging by drop-casting 5 to 15 μL of the NP dispersion onto a carbon-coated Cu TEM grid. NP size distributions were determined by measuring >100 individual NPs from TEM images of each sample using the Nano Measurer 1.2 image analysis software. Within this software, the boundaries of each NP were located manually. Size distribution histograms are available in the Supporting Information, Figure S1.

Molecular Simulations. The surface-adsorbed conformational ensembles of the A3- and AuBP1-based sequences were predicted using Replica Exchange with Solute Tempering (REST)[11-12] molecular dynamics (MD) simulations. We performed a REST-MD simulation for each of the twelve peptide sequences listed in Table 1. Each REST-MD simulation comprised a single peptide chain adsorbed at the Au(111) interface in the presence of liquid water. Earlier studies indicated that the Au(111) surface is a reasonable surrogate for the polycrystalline Au substrate, as used in the QCM experiments.[3, 13-14] Three-dimensional periodic boundary conditions were used throughout. The polarizable GolP-CHARMM force-field,[15-16] the CHARMM22* force-field,[17-18] and the modified TIP3P potential[19-20] were used to describe the interactions involving the Au surface, the peptide, and water, respectively. The GolP-CHARMM force-field has been recently demonstrated to be in good agreement in the near-reproduction of the experimentally-determined binding free energy of the AuBP1 peptide at the aqueous Au interface.[13] We used the Gromacs[21] software package for all of the simulations described herein. All REST-MD simulations were carried out at a thermal temperature of 300 K, using 16 replicas to span "effective temperature" space.[11] Full details regarding the simulation procedures and analysis of the simulation trajectories are provided in the 'Additional Methodology' section of the Supporting Information.

Results and Discussion

QCM Analysis of Peptide Binding to Au. Although the A3 and AuBP1 parent sequences are both Au-binding peptides[22-24] and each possesses three anchor residues for Au-binding,[6-7] AuBP1 is a substantially stronger binder than A3.[6] To analyze the sequence characteristics that affect the kinetics and thermodynamics of binding, a set of five mutant peptide sequences was prepared for each parent biomolecule. QCM measurements quantified the free energy of binding (ΔG) of each peptide of the library for Au surfaces, as shown in Table 1. As an example of the QCM analysis, Figure 1a presents the observed frequency changes for A3-1 at five different peptide concentrations. Higher peptide concentrations yielded faster and larger frequency changes, reflecting increased binding rates and increased amounts of peptide bound to the metallic surface. The dissipation energy, which is indicative of the viscoelasticity of the bound peptide layer, is shown for the highest peptide concentration (15 μg/mL). For all of the peptides studied here, the dissipation energy was observed to be <5% of the total frequency change. This indicates that the absorbed peptide layer was rigidly bound to the Au surface, strongly suggesting that only a single peptide layer was formed. Note that for all QCM data, inverted plots are displayed for more intuitive data interpretation. The QCM analysis for all of the peptides is presented in the Supporting Information, Figures S2-S3.

Pseudo-first-order adsorption rate constants (k_{obs}) were obtained by fitting each QCM binding curve to Langmuir kinetics, as in prior studies.[6, 8-9] The binding constants for adsorption (k_a) and desorption (k_d) are given by the slope and y-intercept, respectively, of the best-fit line obtained by plotting the k_{obs} values as a function of the peptide concentration (Figure 1b). The binding equilibrium constant, K_{eq}, is then calculated as k_a/k_d, and finally, the binding affinity for

peptide binding, defined as the change in ΔG between the bound and unbound states, is determined from $\Delta G = -RT \ln(K_{eq})$. A summary of the k_a, k_d, and K_{eq} values for each peptide in Table 1 can be found in the Supporting Information, Table S1.

For the A3 mutant peptides, the ΔG values ranged from −28.4 to −36.6 kJ/mol for the weakest (A3-5) and strongest (A3-1) binders, respectively. For the parent A3 peptide, a ΔG value of −31.6 ± 0.5 kJ/mol was measured, equivalent to previously reported values.[7] Replacement of the Tyr at position 2 with Ala (*i.e.* the Y2A mutation) in A3-1 produced a substantial increase in binding affinity to –36.6 ± 1.1 kJ/mol. This change is quite surprising in light of the removal of an anchor residue. When the second or third anchor residue was replaced by Ala, as in A3-2 (M9A mutation) and A3-3 (F12A mutation), the binding affinity was reduced, to –28.8 ± 0.9 kJ/mol and –30.5 ± 0.2 kJ/mol, respectively. This suggests that the local context of anchor residues is an influential factor affecting the Au-binding affinity of the peptide. Finally, all further changes, including sequence scrambling or grouping of anchor residues at the N-terminus resulted in diminished Au affinity relative to the parent A3 sequence. A ΔG value of –30.6 ± 0.1 kJ/mol was determined for the A3-4 peptide, while the weakest binding of the set was observed from the A3-5 peptide with a ΔG value of –28.4 ± 0.2 kJ/mol.

Modification of the AuBP1 peptide provided further insights. QCM measurements on the parent sequence gave a ΔG value of –40.7 ± 2.1 kJ/mol, which is similar to previously reported values.[6-7] Note that this peptide sequence represents one of the strongest known binding sequences, based upon experimental quantification, for Au. Each modification to this sequence resulted in a significant reduction in Au affinity. For example, whenever a single anchor residue was replaced by Ala, as in the AuBP1-1 (W1A mutation), AuBP1-2 (R6A mutation), and AuBP1-3 (R11A mutation) peptides, the binding affinity decreased substantially, with ΔG values

of –32.2 ± 0.5 kJ/mol, –35.9 ± 0.7 kJ/mol, and –33.3 ± 0.7 kJ/mol, respectively. This indicates that mutation of the individual anchor residues consistently affected the Au affinity. However, the effect was greatest for the AuBP1-1 and AuBP1-3 sequences, in which the Ala mutation occurred at the N-terminus or the C-terminus, respectively. A dramatic decrease in binding affinity (ΔG = –32.6 ± 0.9 kJ/mol) was also observed for the scrambled sequence, while the AuBP1-5 peptide (anchors grouped together at the N-terminus) exhibited a smaller decrease in binding affinity with a ΔG value of –34.2 ± 0.4 kJ/mol.

Molecular Dynamics Simulations of Peptide Binding to Au. REST-MD simulations were then used to interpret the QCM data *via* prediction of the conformational ensemble of each of the twelve peptide sequences adsorbed at the aqueous Au(111) interface. We first discuss the six A3-based sequences for which the degree of residue-surface contact with the Au surfaces was determined from our simulations, as summarized in Table 2. The parent A3 peptide was predicted to have three anchor residues, Tyr2, Met9, and Phe12 (indicated as red-highlighted entries in Table 2). Intuitively, one might therefore expect that the Y2A mutation (A3-1 sequence) would result in a reduction of Au-binding affinity. However, consistent with the unexpected results from the QCM observations, the enthalpic contribution to the overall peptide binding, as measured by the number and persistence of the resulting anchor residues, appeared to increase, while the surface contact of several non-anchor residues also increased (Table 2). Moreover, the impact of the Y2A mutation appeared to be non-local, producing an increase in surface contact for the central segment of the peptide chain, while the Met9 and Phe12 sites also remained as anchor residues. In contrast with the results for A3-1, the predicted outcomes of the A3-2 mutation (M9A) were more intuitive, resulting in a more spatially-localized impact on

binding compared with the parent peptide. Our residue-surface contact data were consistent with the decrease in binding strength observed using QCM, due to deletion of the Met9 anchor point. The degree of residue-surface contact for all other residues in A3-2 remained broadly invariant to this point mutation.

The sequence arising from F12A mutation, A3-3, resulted in a degree of residue-surface contact that was intermediate between A3-1 and A3-2 (see Table 2), consistent with the experimentally-observed adsorption free energy for A3-3, which was also intermediate between that of A3-1 and A3-2 (Table 1). The randomized sequence, A3-4, also showed reduced binding according to the QCM data, which our simulations suggest may be due to the reduction in binding of Phe10. In the A3 parent and the point mutations (A3-1 and A3-2), Phe was located at position 12 and featured good surface contact (~95% degree of contact on average). This contact was reduced to 49% for A3-4 when Phe was moved to position 10. While the surface contact of Phe was strongly downgraded by the sequence randomization (A3-4), both Tyr1 and Met11 remained as anchors. We propose that the diminishment of Phe-surface contact in A3-4 may be due to the presence of Met as a flanking residue, leading to a reduction in surface binding when two anchors are adjacent in the sequence. This effect was observed in prior work on the Pd4 sequence.[3]

Similarly, a reduction in Phe-surface contact was also noted for A3-5, which again positioned Met and Phe together. The relatively modest residue-surface contact of A3-5 reflected the greatest reduction in the QCM binding strength compared with the parent sequence. In this case, our simulations predicted a substantial reduction in surface contact for both Met2 and Phe3. In the parent A3 sequence and point mutants, Met featured an average ~97% degree of contact, which dropped to 56% in A3-5, while the surface contact for Phe dropped to 54% in the mutant,

relative to 95% in the parent. Following the arguments presented above, we suggest that the reduction in surface contact for Met2 was due to the presence of the flanking anchor (Tyr1). Overall, these surface-contact data suggest a hierarchical influence when two or more of these anchor residues are consecutively positioned, such that the contact of Tyr appeared to be the least susceptible to change (*i.e.* an adjacent Tyr might reduce Met-surface contact, but not *vice-versa*), while Phe appeared to be the most vulnerable of these three anchors to sequence context effects.

Collectively, we attribute the observed trends in binding properties in part to the conformational response of A3 to the selected point mutations and sequence rearrangements. In addition to probing the changes in residue-surface contact, we also quantified and compared the degree of structural similarity of the peptide backbone conformations for each of the six A3-based peptides adsorbed at the Au interface (see Methodology, and Table S2, Supporting Information). We found that A3-1, A3-2, and A3-3 (the three point mutations) featured remarkable similarity in backbone conformation compared with the parent peptide in the adsorbed state.[6] This conformational recalcitrance to point mutations was also noted for the Pd-4 sequence reported previously.[3] In contrast, the global rearrangements of A3 (A3-4 and A3-5), shared very little backbone conformational similarity. Again, the conformational responses to these global sequence rearrangements was very similar to those reported previously for the Pd4 sequence. To illustrate this point, in Figure 2 we provide the most likely Au-adsorbed structures for each of the six sequences, bearing in mind that each sequence supports a complex *ensemble* of conformations. To briefly explain, our analysis can identify the set of structurally-distinct backbone conformations along with their relative proportions (populations) in the conformational ensemble. A large number of distinct structures with low populations therefore indicates a high

degree of conformational diversity in the ensemble. Details of the number of distinct structures and their relative populations are provided in Table S3 of the Supporting Information.

The similarities in conformational response for both Pd4 and A3 suggest a common trait in these two peptides. However, the variations of the AuBP1 sequence resulted in very different outcomes, both in terms of surface contact and conformational response. Our simulations indicated a reduction in overall peptide-surface contact for all AuBP1 mutants compared with the parent sequence (Table 3). Moreover, the QCM data indicate that AuBP1-1 and AuBP1-4 suffered the greatest reduction in adsorption free energy on the Au surface. As our residue-surface contact data indicate (Table 3), these two sequences also suffered substantial losses in surface contact relative to the parent, particularly for the (remaining) anchors of the parent sequence. For example, in AuBP1-1, the W1A mutation not only resulted in a massive reduction in surface contact at position 1 (reduced to ~14% of the original value), but also diminished surface contact for anchor Arg11, distant from the site of the point mutation. The variant that supported the least reduction in surface binding, AuBP1-2, also featured the least reduction in predicted residue-surface contact, with no appreciable drop in surface contact seen for the remaining anchor residues (Table 3).

In Figure 3, we show the most likely structures of the six AuBP1-based peptides adsorbed at the aqueous Au interface. From these data, in partnership with a mathematical comparison of the structural similarity of the peptide backbone conformations (Table S4, Supporting Information), we found that the AuBP1 mutants shared very little commonality in terms of backbone conformations. This finding indicates that, unlike the Pd4[3] and A3 sequences, AuBP1 is a conformationally-susceptible biomolecule that (in some instances) produced a dramatic conformational response to point mutations. Details of the number of distinct structures

for the AuBP1-based peptides, and their relative populations, are provided in Table S5 of the Supporting Information.

Overall, our predictions from the REST-MD simulations are consistent with the QCM measurements of peptide binding strength. Based on our conformational comparisons reported here and previously,[3] we propose two classes of materials-binding peptide sequences: conformationally-recalcitrant sequences, for which the conformational ensemble of adsorbed structures does not change appreciably for point mutations, and conformationally-susceptible peptides, which can undergo substantial, non-localized changes to backbone conformations upon point mutation. While the general applicability of this proposed categorization requires further investigation, our findings (reported here and in prior work[3]) suggest that the presence of Pro in a sequence may be indicative of conformational-recalcitrance. On this basis, we anticipate that other sequences that bind to Au surfaces and which contain substantial Pro content, such as B1 (LKAHL**PP**SRL**P**S)[25-26] and QBP1 (**PPP**WL**P**YM**PP**WS)[27] may also exhibit conformational recalcitrance, and would likely provide a fruitful test-set for future mutation-based binding investigations.

Au Nanoparticle Synthesis and Characterization. Figures 4a and 5 present UV-vis absorbance spectra and TEM images, respectively, for the Au NPs synthesized using the A3 peptide and designed mutant sequences. The synthesis protocol was the same as that used with the Pd4 peptide in our prior study,[3] where samples for TEM imaging were prepared ~1 h after NP synthesis. The A3 parent and four of the mutant peptides produced small and spherical Au NPs of ~2-3 nm in diameter that exhibited well-defined localized surface plasmon resonance (LSPR) peaks at ~520 nm. Interestingly, the A3-2 mutant peptide produced larger, somewhat irregular NPs and clusters that exhibited a slightly red-shifted and broadened, but also more intense, LSPR

peak. Although A3-2 has a reduced binding affinity, compared to A3, it does not have the lowest binding affinity in the group. A3-5, which has even lower binding affinity, also has notably slower binding kinetics than A3-2 (Supporting Information, Table S1) and a much different conformation on the surface (Figure 2, Table 2) compared to A3-2. A3-2 features two anchor residues that are spaced at opposite ends of the sequence, while A3-5 features only one anchor at position 1. This spatial constraint in A3-2 surface contact may limit the ability of A3-2 to cap very small NPs during growth. As illustrated in Figure 2, the footprint of A3-2 on the Au surface is larger than that of A3-5, thus requiring a larger Au surface area for binding.

Long-term colloidal stability testing showed some variability, as discussed further below, but the most consistent results are considered first. Au NPs capped with the A3-4 peptide were initially well dispersed, as seen in the inset of Figure 4a, approximately one hour after synthesis, but routinely showed signs of precipitation within hours to days after the synthesis. This is consistent with the aggregation of the A3-4 capped NPs visible in the TEM image of Figure 5. While two anchor residues were conserved in A3-4, allowing it to passivate and stabilize the Au NPs during synthesis, the substantially reduced residue-surface contact of Phe10 that arises from sequence randomization may have significantly impaired its conformational advantage in fostering NP stability. This presents an interesting contrast with the A3-2 capped particles, which were larger and more irregular than the other materials, but remained stably dispersed in all experiments. Thus, A3-2 was less able to cap the particles and limit their growth during the rapid synthesis process, compared to the other sequences, but was nonetheless able to stabilize the NP dispersion. A3-4 was able to limit NP growth during synthesis, but was not able to stabilize the NP dispersion as well as the other sequences. Note that the aggregates visible in the TEM image of A3-4 capped NPs in Figure 5 are not primarily made up of Au NPs in direct contact with one

another, but show Au NPs linked together in a matrix. Thus, the precipitation may reflect aggregation of peptide-capped NPs due to peptide-peptide interactions between individual NPs, rather than aggregation of Au NPs with one another at points where the Au surface is exposed (due to peptide desorption or low coverage). Note that, as shown in Figure 2, the dominant conformation of A3-4 on the Au surface is quite different from that of the other peptides. Thus, it may present a different exterior surface to the surrounding solution. Regarding the overall hydrophobicity and solubility of the mutant sequences, while our estimates of the peptide hydropathy for each sequence (Table S6, Supporting Information) showed some variation, none of these values indicated any severe problems with hydrophobicity.

We investigated this further *via* examination of the REST-MD trajectory of A3-4 in the surface-adsorbed state. As indicated in Table 2, Phe10 is not strongly engaged with the surface, spending about half of the trajectory projected away from the surface, and the other half of the trajectory in contact with the surface (illustrated in Figure 2). In Figure 6 we provide a representative structure of an additional configuration (which is also predicted to be highly likely), in which Phe10 protrudes away from the surface and into the surrounding solution, along with the exposure of additional hydrophobic residues (Pro2, Ala4, and Ala7) to the solvent. We suggest the external presentation of these hydrophobic residues may be conducive to the formation of bridging inter-peptide interactions between the Au NPs in solution, particularly for the exposed Phe10, which might facilitate specific inter-particle π–π bridging interactions.

Au NPs capped with the A3-1 and A3-5 mutants, like those capped with A3-2, remained stably dispersed in all experiments. Thus, in these two cases, the peptide was not only able to limit NP growth during synthesis, but also cap the NPs and maintain colloidal stability. Surprisingly, the parent peptide, A3, and the A3-3 mutant gave inconsistent results, in some

cases producing NPs that precipitated after hours to days, while in other, nominally identical, experiments producing dispersions that remained stable for more than a week. Although A3 (or chimeric molecules that incorporate this sequence) has been used to produce peptide-capped particles in many other studies,[28-30] it has generally been used in HEPES buffer, which maintains a pH near 7.4. Additionally, in those synthetic methods, the HEPES buffer also acted as the reductant. In our protocol, we synthesize the NPs in pure water, without buffering the pH, employing $NaBH_4$ to reduce the Au^{3+} ions to Au^0. In the absence of a buffer, the gold precursor used in the synthesis produces slightly acidic conditions after the reaction, and the stability of Au NPs capped with A3 and A3-3 appears to be highly sensitive to pH. For cases in which the A3-capped NPs precipitated, adding a small amount of NaOH allowed us to redisperse the materials. When a metal:peptide ratio higher than the usual value of 3:1 was employed, A3 consistently produced colloidally unstable particles and the product dispersion had a significantly acidic pH (near 5). When a lower metal:peptide ratio of 1:1 was employed, the Au NPs were consistently stable. Addition of excess reducing agent ($NaBH_4$) relative to our standard protocol also improved colloidal stability. While many factors are at play here, and complete investigation of them is beyond the scope of the present study, together the results show that all of the A3 mutants except for A3-4 are capable of producing colloidally stable dispersions of peptide-capped Au NPs, but in some cases the stability is highly sensitive to solution and reaction conditions.

Similarly, AuBP1 and its mutants were used to synthesize Au NPs, as presented in Figures 4b and 7. The AuBP1-1 and AuBP1-3 peptides showed a reduced ability to cap and stabilize the Au NPs during nucleation and growth, as reflected in the TEM images. These two sequences exhibited relatively weaker binding affinities in QCM experiments with only a single

anchor residue predicted from molecular simulations, which is consistent with the observed poor performance in NP stabilization. However, AuBP1-4 and AuBP1-5 exhibited similar reductions in binding affinity, relative to the parent sequence; each of these sequences also featured only one anchor residue, but still produced Au NPs almost identical to those generated with the more strongly-bound parent AuBP1 and AuBP1-2 that have three and two anchor residues, respectively. The difference between the results for AuBP1-1 and AuBP1-3 *vs*. AuBP1-4 and AuBP1-5 may reflect the larger footprint of AuBP1-1 and AuBP1-3 on the Au NP surface compared to AuBP1-4 and AuBP1-5, where in the latter, each has segments of several consecutive residues with very low binding probability.

The Au NP dispersions produced using the AuBP1 parent peptide and the AuBP1-4 and AuBP1-5 mutants remained colloidally stable with no signs of precipitation for at least a week in all cases. In contrast, the Au NP dispersion produced using AuBP1-1 consistently began to show signs of aggregation and precipitation after a few hours post reduction, and the Au NPs had almost completely precipitated after 24 h. The NPs produced using AuBP1-2 and AuBP1-3 precipitated in some experiments, but in most cases were also colloidally stable. We suggest that this outcome might again be due to the sensitivity of this precipitation process to the precise solution conditions. As with the results for A3 discussed above, this may reflect sensitivity to pH and other solution conditions. The TEM images of the NPs produced using AuBP1-1 and AuBP1-3, prepared from dispersions about 1 h after synthesis, show clear signs of aggregation. In the case of AuBP1-1, the Au NPs are not only large and irregular, but also significantly aggregated, with direct particle-particle contacts, suggesting that AuBP1-1 was unable to effectively passivate the Au NPs during synthesis. The Au NPs produced using AuBP1-3 also showed aggregation, but this case is similar to that observed for materials produced with A3-4.

Rather than showing direct particle-particle contacts in aggregates, the Au NPs seem to be embedded in a matrix, suggesting possible aggregation through peptide-peptide interactions. Little aggregation of the Au NPs prepared using AuBP1-2 is visible in the TEM image. These Au NPs look quite similar to those in the colloidally stable dispersions produced using AuBP1, but in some experiments precipitated nonetheless. This again demonstrates that the requirements for limiting NP growth and capping the materials may be different from the requirements for stabilizing the aqueous dispersion of NPs.

From the NP synthesis and characterization analyses, no direct correlation between NP colloidal stability, final particle sizes, and peptide binding affinity is apparent. We found that both large and small nanoparticles were capable of supporting a stable colloidal dispersion. For instance, the A3-1 peptide possessed the highest binding affinity for Au of all of the A3-based peptides, yet it generated the particles with the largest average size (Figure 1). Furthermore for this system, the A3-4 peptide produced particles that precipitated, even though this peptide is of intermediate strength for Au binding under the present conditions. In these examples, one might intuitively assume that the A3-1 should generate the smallest particles, while the A3-4, with the weakest affinity for Au should generate the largest particles. However, such a pattern was not observed. These two examples demonstrate the lack of correlation between particle size, colloidal stability, and peptide affinity, suggesting that other factors must participate and work synergistically to control the morphology of the final materials. Such factors could include key atomic structural motifs recognized by the peptide for binding,[31] the rate of NP growth based upon the reductant selected,[32] the number and spacing of anchor residues within the peptide sequence,[5] as well as other factors. By identifying and eventually tuning these different

contributions, highly controlled particle synthesis strategies could be realized and exploited for rational design of NPs.

As introduced in earlier work,[3] we propose that one possible mechanism for promoting peptide-mediated stabilization of Au NP dispersions in aqueous media may arise from the presence of a high degree of conformational diversity in the NP-adsorbed peptide structures. As previously reported, here we have used our definition of the conformational entropic contribution, S_{conf} (details in 'Additional Methodology' of the Supporting Information), to estimate the degree of conformational diversity in the adsorbed peptide structures. In Figure 8 (and Tables S3 and S5 of the Supporting Information) we summarize our predictions of S_{conf} alongside our previously-published data for the Pd4-based sequences for convenience. These data suggest critical upper and lower thresholds for peptide-mediated stabilization/precipitation. Specifically, we propose that surface-adsorbed peptides with $S_{conf} > S_{conf}^{high}$ have a strong likelihood to cause Au NP precipitation, while those peptides with $S_{conf} < S_{conf}^{low}$ are likely to stabilize Au NP dispersion in aqueous media. We identified the range of values of S_{conf}^{high} and S_{conf}^{low} based on our previous work.[3, 5-7, 33] The range of values between S_{conf}^{high} and S_{conf}^{low} represents an uncertainty band for which we suggest that the outcomes cannot be predicted with confidence. Figure 8 also highlights the four systems with the most inconsistency in terms of the NP stabilization assay, where the degree of confidence in our predictions is low.

Our proposed classification based on S_{conf} values appears broadly consistent with the experimental data, in the sense that NPs that showed reasonably consistent stabilization behaviors (*i.e.* that were consistently stable or consistently unstable) were captured by our analysis. However, our metric was unable to capture inconsistent NP stabilization scenarios. We

note here that our S_{conf} metric is an approximation based on single-chain adsorption properties (*i.e.* corresponding to dilute conditions), and therefore it is not surprising that it cannot cover all possible situations. For example, as suggested earlier, in some instances surface-driven inter-peptide interactions are likely to influence stabilization. For the AuBP1 sequences in particular, inter-chain interactions in the surface-adsorbed state of the peptides may lead to deviations from our idealized conditions. To elaborate, unlike the Pd4 or A3 sequences, AuBP1 features several charged residues in solution at pH≈7, comprising a positively-charged Lys and three Arg residues, and a negatively-charged Asp. Evidence drawn from previous studies of multi-chain NP-adsorbed AuBP1 peptides[5] suggests that inter-chain interactions involving oppositely-charged residues could be substantial. Further study is required to resolve the possible origins of the inconsistent stabilization properties for the four systems identified here. While pH-based mechanisms offer a plausible hypothesis, several mechanisms governing Au NP dispersion/precipitation are likely to co-exist, and remain to be proposed and tested in future work.

Conclusions

By combining peptide-surface binding affinity measurements, nanoparticle synthesis, characterization and stabilization assays, and advanced molecular simulations, we have identified new factors that influence both Au nanoparticle growth and nanoparticle colloidal stability in aqueous media. Colloidal stability is defined here as the absence of visible precipitation after at least 24 hours post-synthesis. We based our investigation on two peptides with strong affinity for Au, considering both point mutations and re-ordering of these sequences. Our findings demonstrate that a strong Au nanoparticle peptide binding affinity does not always guarantee

peptide-mediated colloidal stability. Instead, by comparing nanoparticle stabilization assay outcomes with molecular simulations, we established a metric that is broadly indicative of nanoparticle colloidal stability, based on the degree of conformational diversity in the surface-adsorbed peptides. While our results offer guidance on the engineering of peptide sequences to realize peptide-mediated growth and dispersion of Au nanoparticles in aqueous media, alternative mechanisms governing colloidal stability are further required to comprehensively encompass the complex phenomena of peptide-based nanoparticle growth and stabilization.

Acknowledgments: This material is based upon work supported by the Air Office of Scientific Research, grant number FA9550-12-1-0226. We gratefully acknowledge the Victorian Life Sciences Computation Facility (VLSCI) for allocation of computational resources.

Supporting Information: Additional methodological details, binding constants for the A3 and AuBP1 mutant peptides, QCM analysis, size distribution histograms, structural similarity analyses, and conformational analyses. This material is available free of charge *via* the Internet at http://pubs.acs.org.

Notes: Current address for M.A.N is Department of Biomedical Engineering, University of Miami, FL, USA. Current address for Z.E.H is School of Chemistry and Biosciences, University of Bradford, Bradford, BD7 1DP, UK.

References

(1) Walsh, T. R.; Knecht, M. R., Biointerface Structural Effects on the Properties and Applications of Bioinspired Peptide-Based Nanomaterials. *Chem. Rev.,* **2017,** *117*, 12641-12704.
(2) Tan, Y. N.; Lee, J. Y.; Wang, D. I. C. Uncovering the Design Rules for Peptide Synthesis of Metal Nanoparticles. *J. Amer. Chem. Soc.* **2010,** *132*, 5677-5686.
(3) Hughes, Z. E.; Nguyen, M. A.; Li, Y.; Swihart, M. T.; Walsh, T. R.; Knecht, M. R. Elucidating the Influence of Materials-Binding Peptide Sequence on Au Surface Interactions and Colloidal Stability of Au Nanoparticles. *Nanoscale,* **2017,** *9*, 421-432.
(4) Yu, Y.; Mok, B. Y. L.; Loh, X. J.; Tan, Y. N. Rational Design of Biomolecular Templates for Synthesizing Multifunctional Noble Metal Nanoclusters toward Personalized Theranostic Applications. *Adv. Healthc. Mater.,* **2016,** *5*, 1844-1859.
(5) Bedford, N. M.; Hughes, Z. E.; Tang, Z. H.; Li, Y.; Briggs, B. D.; Ren, Y.; Swihart, M. T.; Petkov, V. G.; Naik, R. R.; Knecht, M. R.; Walsh, T. R. Sequence-Dependent Structure/Function Relationships of Catalytic Peptide-Enabled Gold Nanoparticles Generated under Ambient Synthetic Conditions. *J. Amer. Chem. Soc.,* **2016,** *138*, 540-548.
(6) Tang, Z. H.; Palafox-Hernandez, J. P.; Law, W. C.; Hughes, Z. E.; Swihart, M. T.; Prasad, P. N.; Knecht, M. R.; Walsh, T. R. Biomolecular Recognition Principles for Bionanocombinatorics: An Integrated Approach to Elucidate Enthalpic and Entropic Factors. *ACS Nano,* **2013,** *7*, 9632-9646.
(7) Palafox-Hernandez, J. P.; Tang, Z. H.; Hughes, Z. E.; Li, Y.; Swihart, M. T.; Prasad, P. N.; Walsh, T. R.; Knecht, M. R. Comparative Study of Materials-Binding Peptide Interactions with Gold and Silver Surfaces and Nanostructures: A Thermodynamic Basis for Biological Selectivity of Inorganic Materials. *Chem. Mater.,* **2014,** *26*, 4960-4969.
(8) Tamerler, C.; Oren, E. E.; Duman, M.; Venkatasubramanian, E.; Sarikaya, M. Adsorption Kinetics of an Engineered Gold Binding Peptide by Surface Plasmon Resonance Spectroscopy and a Quartz Crystal Microbalance. *Langmuir,* **2006,** *22*, 7712-7718.
(9) Tamerler, C.; Duman, M.; Oren, E. E.; Gungormus, M.; Xiong, X. R.; Kacar, T.; Parviz, B. A.; Sarikaya, M. Materials Specificity and Directed Assembly of a Gold-Binding Peptide. *Small,* **2006,** *2*, 1372-1378.
(10) Li, Y.; Tang, Z. H.; Prasad, P. N.; Knecht, M. R.; Swihart, M. T. Peptide-Mediated Synthesis of Gold Nanoparticles: Effects of Peptide Sequence and Nature of Binding on Physicochemical Properties. *Nanoscale,* **2014,** *6*, 3165-3172.
(11) Terakawa, T.; Kameda, T.; Takada, S. On Easy Implementation of a Variant of the Replica Exchange with Solute Tempering in GROMACS. *J. Comput. Chem.* **2011,** *32*, 1228-1234.
(12) Wright, L. B.; Walsh, T. R. Efficient Conformational Sampling of Peptides Adsorbed onto Inorganic Surfaces: Insights from a Quartz Binding Peptide. *Phys. Chem. Chem. Phys.,* **2013,** *15*, 4715-4726.
(13) Wright, L. B.; Palafox-Hernandez, J. P.; Rodger, P. M.; Corni, S.; Walsh, T. R. Facet Selectivity in Gold Binding Peptides: Exploiting Interfacial Water Structure. *Chem. Sci.,* **2015,** *6*, 5204-5214.
(14) Kochandra, R.; Hughes, Z. E.; Walsh, T. R. Facet-Specific Adsorption of Tri-Peptides at Aqueous Au Interfaces: Reconciling Experiment and Simulation. *Langmuir,* **2017,** *33*, 3742-3754.

(15) Wright, L. B.; Rodger, P. M.; Corni, S.; Walsh, T. R. GolP-CHARMM: First-Principles Based Force Fields for the Interaction of Proteins with Au(111) and Au(100). *J. Chem. Theory Comput.,* **2013,** *9*, 1616-1630.
(16) Wright, L. B.; Rodger, P. M.; Walsh, T. R.; Corni, S. First-Principles-Based Force Field for the Interaction of Proteins with Au(100)(5×1): An Extension of GolP-CHARMM. *J. Phys. Chem. C,* **2013,** *117*, 24292-24306.
(17) MacKerell, A. D.; Bashford, D.; Bellott, M.; Dunbrack, R. L.; Evanseck, J. D.; Field, M. J.; Fischer, S.; Gao, J.; Guo, H.; Ha, S.; Joseph-McCarthy, D.; Kuchnir, L.; Kuczera, K.; Lau, F. T. K.; Mattos, C.; Michnick, S.; Ngo, T.; Nguyen, D. T.; Prodhom, B.; Reiher, W. E.; Roux, B.; Schlenkrich, M.; Smith, J. C.; Stote, R.; Straub, J.; Watanabe, M.; Wiórkiewicz-Kuczera, J.; Yin, D.; Karplus, M. All-Atom Empirical Potential for Molecular Modeling and Dynamics Studies of Proteins. *J. Phys. Chem. B,* **1998,** *102*, 3586-3616.
(18) Piana, S.; Lindorff-Larsen, K.; Shaw, D. E. How Robust Are Protein Folding Simulations with Respect to Force Field Parameterization? *Biophys. J.,* **2011,** *100*, L47-L49.
(19) Jorgensen, W. L.; Chandrasekhar, J.; Madura, J. D.; Impey, R. W.; Klein, M. L. Comparison of Simple Potential Functions for Simulating Liquid Water. *J. Chem. Phys.,* **1983,** *79*, 926-935.
(20) Neria, E.; Fischer, S.; Karplus, M., Simulation of Activation Free Energies in Molecular Systems. *J. Chem. Phys.,* **1996,** *105*, 1902-1921.
(21) Wennberg, C. L.; Murtola, T.; Pall, S.; Abraham, M. J.; Hess, B.; Lindahl, E. Direct-Space Corrections Enable Fast and Accurate Lorentz-Berthelot Combination Rule Lennard-Jones Lattice Summation. *J. Chem. Theory Comput.,* **2015,** *11*, 5737-5746.
(22) Naik, R. R.; Stringer, S. J.; Agarwal, G.; Jones, S. E.; Stone, M. O. Biomimetic Synthesis and Patterning of Silver Nanoparticles. *Nat. Mater.,* **2002,** *1*, 169-172.
(23) Lu, Z. J.; Murray, K. S.; Vancleave, V.; Lavallie, E. R.; Stahl, M. L.; Mccoy, J. M. Expression of Thioredoxin Random Peptide Libraries on the Escherichia-Coli Cell-Surface as Functional Fusions to Flagellin - a System Designed for Exploring Protein-Protein Interactions. *Bio-Technol.,* **1995,** *13*, 366-372.
(24) Hnilova, M.; Oren, E. E.; Seker, U. O. S.; Wilson, B. R.; Collino, S.; Evans, J. S.; Tamerler, C.; Sarikaya, M. Effect of Molecular Conformations on the Adsorption Behavior of Gold-Binding Peptides. *Langmuir,* **2008,** *24*, 12440-12445.
(25) Whaley, S. R.; English, D. S.; Hu, E. L.; Barbara, P. F.; Belcher, A. M. Selection of Peptides with Semiconductor Binding Specificity for Directed Nanocrystal Assembly. *Nature,* **2000,** *405*, 665-668.
(26) Nam, K. T.; Wartena, R.; Yoo, P. J.; Liau, F. W.; Lee, Y. J.; Chiang, Y. M.; Hammond, P. T.; Belcher, A. M. Stamped Microbattery Electrodes Based on Self-Assembled M13 Viruses. *P. Natl. Acad. Sci. USA,* **2008,** *105*, 17227-17231.
(27) Oren, E. E.; Tamerler, C.; Sahin, D.; Hnilova, M.; Seker, U. O. S.; Sarikaya, M.; Samudrala, R. A Novel Knowledge-Based Approach to Design Inorganic-Binding Peptides. *Bioinformatics,* **2007,** *23*, 2816-2822.
(28) Slocik, J. M.; Stone, M. O.; Naik, R. R. Synthesis of Gold Nanoparticles Using Multifunctional Peptides. *Small,* **2005,** *1*, 1048-1052.
(29) Slocik, J. M.; Naik, R. R. Biologically Programmed Synthesis of Bimetallic Nanostructures. *Adv. Mater.,* **2006,** *18*, 1988-1992.
(30) Chen, C. L.; Zhang, P. J.; Rosi, N. L. A New Peptide-Based Method for the Design and Synthesis of Nanoparticle Superstructures: Construction of Highly Ordered Gold Nanoparticle Double Helices. *J. Amer. Chem. Soc.,* **2008,** *130*, 13555-13557.

(31) Coppage, R.; Slocik, J. M.; Briggs, B. D.; Frenkel, A. I.; Heinz, H.; Naik, R. R.; Knecht, M. R., Crystallographic Recognition Controls Peptide Binding for Bio-Based Nanomaterials. *J. Amer. Chem. Soc.* **2011,** *133*, 12346-12349.
(32) Briggs, B. D.; Li, Y.; Swihart, M. T.; Knecht, M. R. Reductant and Sequence Effects on the Morphology and Catalytic Activity of Peptide-Capped Au Nanoparticles. *ACS Appl. Mater. Interfaces,* **2015,** *7*, 8843-8851.
(33) Sultan, A. M.; Westcott, Z. C.; Hughes, Z. E.; Palafox-Hernandez, J. P.; Giesa, T.; Puddu, V.; Buehler, M. J.; Perry, C. C.; Walsh, T. R. Aqueous Peptide-TiO_2 Interfaces: Isoenergetic Binding Via Either Entropically or Enthalpically Driven Mechanisms. *ACS Appl. Mater. Interfaces,* **2016,** *8*, 18620-18630.

Figure/Table Captions

Table 1. Adsorption Analysis for A3 and AuBP1 Mutant Peptides on Au[a]

Table 2. Degree of residue-surface contact (expressed as a percentage) for each of the six A3-based peptide sequences, adsorbed at the aqueous Au interface, predicted from REST simulations. White, blue, green, orange, and red cell colors indicate 0-19%, 20-39%, 40-59%, 60-79%, and 80+% contact, respectively.

Table 3. Degree of residue-surface contact (expressed as a percentage) for each of the six AuBP1-based peptide sequences, adsorbed at the aqueous Au interface, predicted from REST simulations. White, blue, green, orange, and red cell colors indicate 0-19%, 20-39%, 40-59%, 60-79%, and 80+% contact, respectively.

Figure 1. QCM analysis of peptide binding on Au to obtain k_a and k_d values. For this example, the A3-1 peptide was used. Part (a) shows the inverted frequency change *vs.* time plot for five concentrations, as well as the dissipation energy plot for the highest concentration studied. Part (b) shows k_{obs} values *vs.* peptide concentration, obtained from the data in part (a) by fitting using Langmuir kinetics. Note that no error bars are presented as they are smaller than the points in the graph. The slope and *y*-intercept in part (b) provide the rate constants for adsorption and desorption, respectively.

Figure 2. Most likely structures of the six indicated A3-based peptides adsorbed at the aqueous Au interface, predicted from the REST simulations. Water not shown for clarity.

Figure 3. Most likely structures of the six indicated AuBP1-based peptides adsorbed at the aqueous Au interface, predicted from the REST simulations. Water not shown for clarity.

Figure 4. UV-vis absorbance spectra of the Au NPs prepared using the (a) A3 peptide and its mutants and (b) AuBP1 peptide and its mutants. Insets show images of the corresponding colloidal dispersions, approximately 1 h after synthesis.

Figure 5. Representative TEM images of Au NPs prepared using the A3 peptide and its mutants, as labelled.

Figure 6. Representative conformation of A3-4 adsorbed at the aqueous Au interface, in the instance where F10 is not in surface contact. Solvent-exposed hydrophobic residues P2, A4, A7 and F10 are highlighted in green, while anchor residues Y1 and M11 are highlighted in red. Water not shown for clarity.

Figure 7. Representative TEM images of Au NPs prepared using the AuBP1 peptide and its mutants, as labelled. Note the different magnification used for AuBP1-1 and AuBP1-3 to highlight the degree of aggregation in these systems.

Figure 8. Conformational entropic contributions to the binding (S_{conf}) calculated from REST-MD simulations. Green and red indicate stable and unstable Au NP dispersions as observed from experiment. Beige bars indicate systems that exhibited the most inconsistency in the nanoparticle

stabilization experiments. S_{conf}^{low} and S_{conf}^{high} correspond with values 3.10 and 3.28 respectively. Pd4 data were taken from Ref 3.

Peptide	Sequence	ΔG (kJ mol^{-1})
A3	AYSSGAPPMPPF	-31.6 ± 0.5
A3-1	AASSGAPPMPPF	-36.6 ± 1.1
A3-2	AYSSGAPPAPPF	-28.8 ± 0.9
A3-3	AYSSGAPPMPPA	-30.5 ± 0.2
A3-4	YPPAPSAPSFMG	-30.6 ± 0.1
A3-5	YMFASSGAPPPP	-28.4 ± 0.2
AuBP1	WAGAKRLVLRRE	-40.7 ± 2.1
AuBP1-1	AAGAKRLVLRRE	-32.2 ± 0.5
AuBP1-2	WAGAKALVLRRE	-35.9 ± 0.7
AuBP1-3	WAGAKRLVLRAE	-33.3 ± 0.7
AuBP1-4	ALRWVGRRAELK	-32.6 ± 0.0
AuBP1-5	WRRAGAKLVLRE	-34.2 ± 0.4

[a]From QCM experiments: adsorption Gibbs free energy (ΔG) values are given as mean ± one standard deviation from at least three independent experiments.

Table 1. Nguyen *et al.*

A3		A3-1		A3-2		A3-3		A3-4		A3-5	
A	3	A	16	A	2	A	2	Y	92	Y	94
Y	98	A	42	Y	97	Y	98	P	8	M	56
S	23	S	39	S	40	S	24	P	6	F	54
S	58	S	53	S	63	S	75	A	48	A	32
G	62	G	90	G	65	G	86	P	23	S	37
A	73	A	79	A	68	A	76	S	40	S	45
P	41	P	78	P	51	P	69	A	37	G	81
P	17	P	20	P	11	P	16	P	56	A	68
M	96	M	96	A	30	M	98	S	31	P	56
P	45	P	40	P	30	P	50	F	49	P	20
P	6	P	1	P	7	P	14	M	97	P	20
F	95	F	97	F	92	A	57	G	47	P	24

Table 2. Nguyen *et al.*

AuBP1		AuBP1-1		AuBP1-2		AuBP1-3		AuBP1-4		AuBP1-5	
W	88	A	12	W	91	W	93	A	11	W	75
A	45	A	37	A	12	A	32	L	35	R	45
G	64	G	50	G	39	G	43	R	70	R	68
A	63	A	48	A	17	A	54	W	90	A	19
K	23	K	19	K	27	K	16	V	23	G	69
R	92	R	85	A	56	R	71	G	70	A	38
L	44	L	33	L	38	L	58	R	65	K	26
V	42	V	63	V	23	V	45	R	66	L	5
L	50	L	40	L	45	L	33	A	17	V	14
R	76	R	74	R	77	R	71	E	33	L	43
R	85	R	53	R	84	A	42	L	16	R	82
E	50	E	25	E	51	E	21	K	6	E	29

Table 3. Nguyen *et al*.

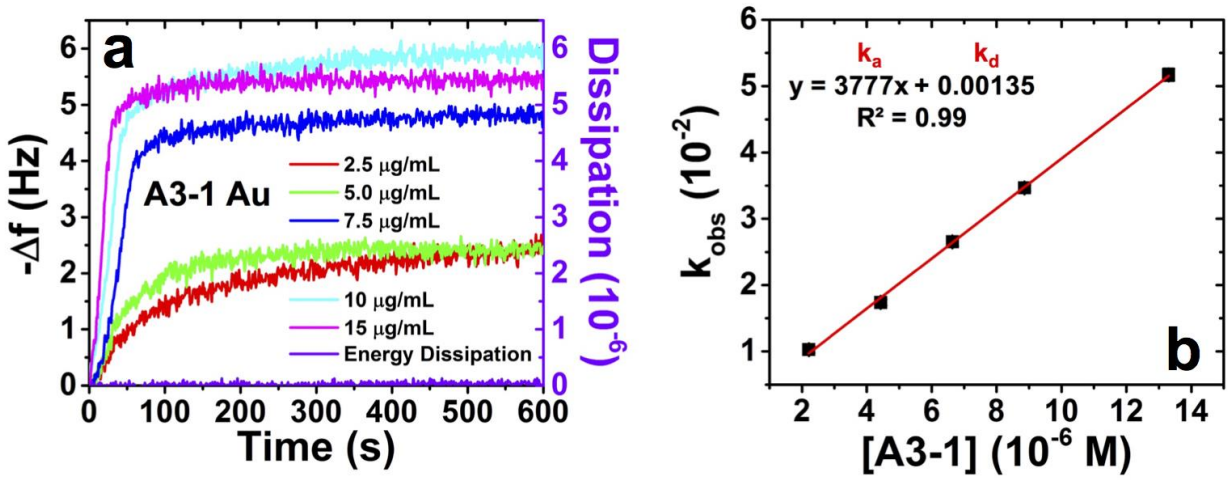

Figure 1. Nguyen *et al*.

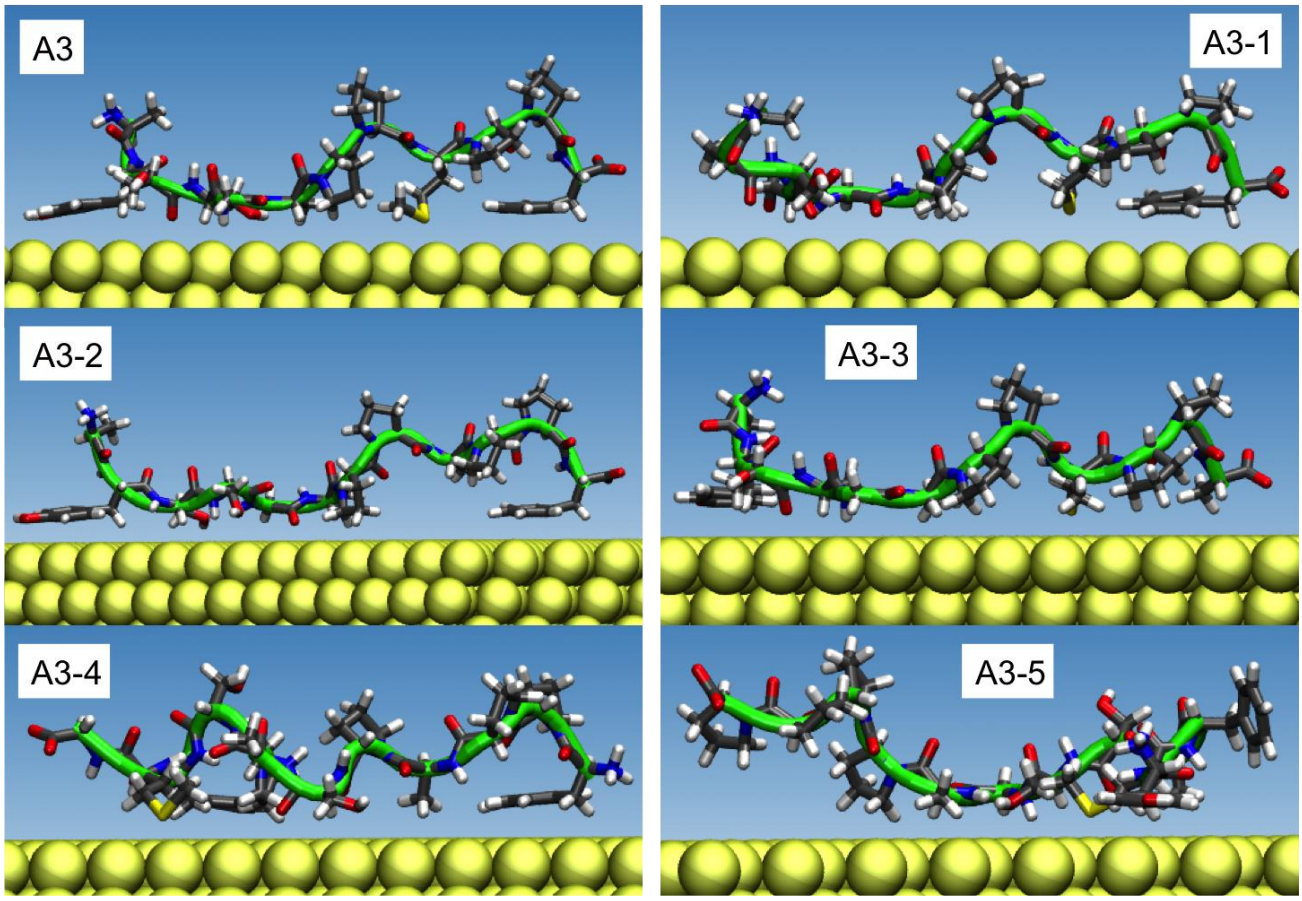

Figure 2. Nguyen *et al*.

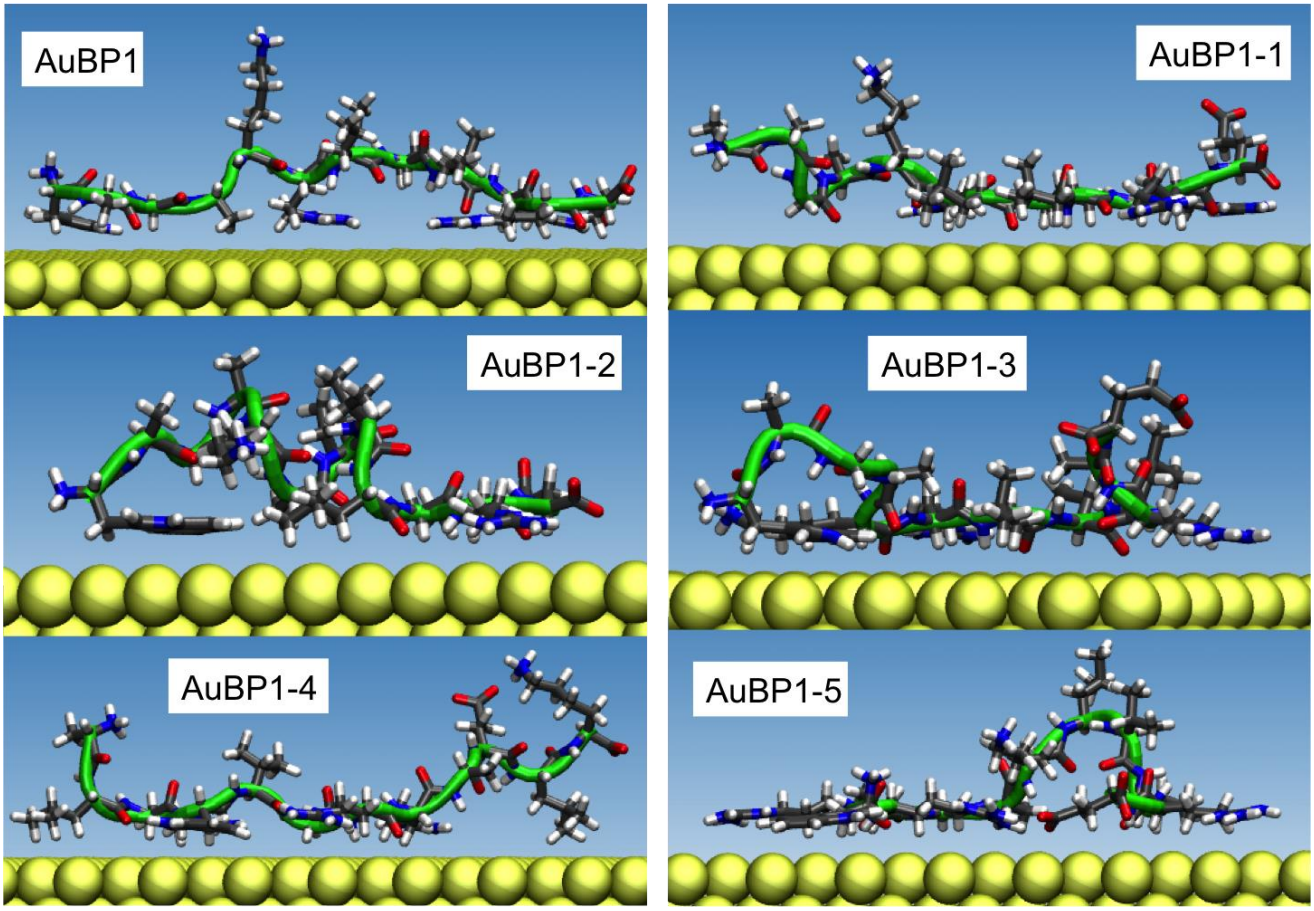

Figure 3. Nguyen *et al*.

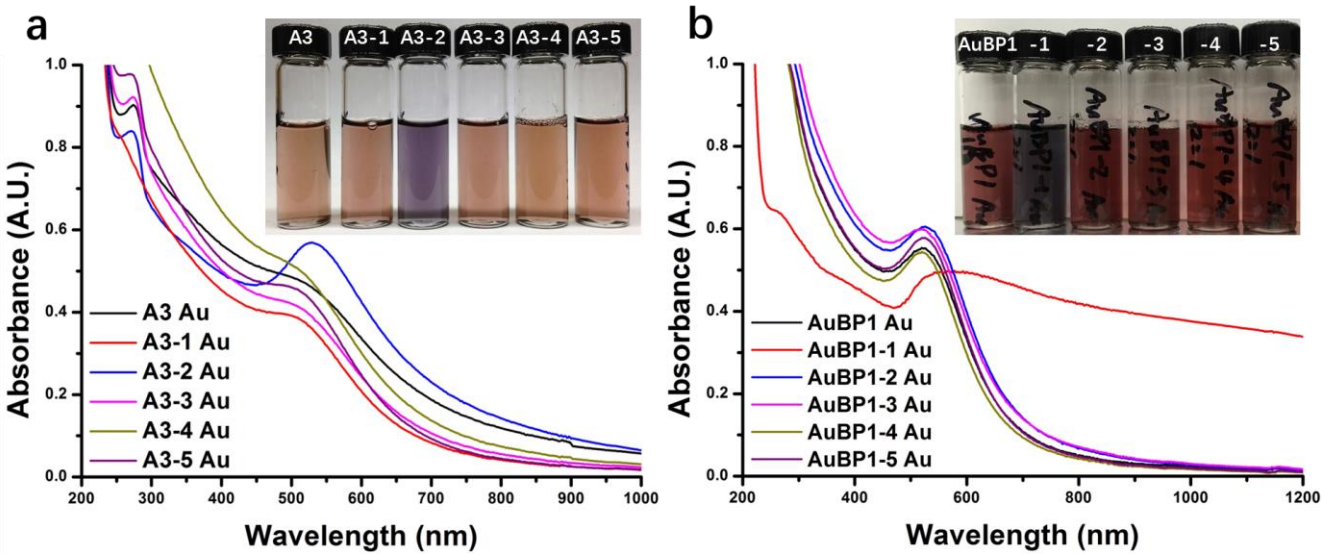

Figure 4. Nguyen *et al.*

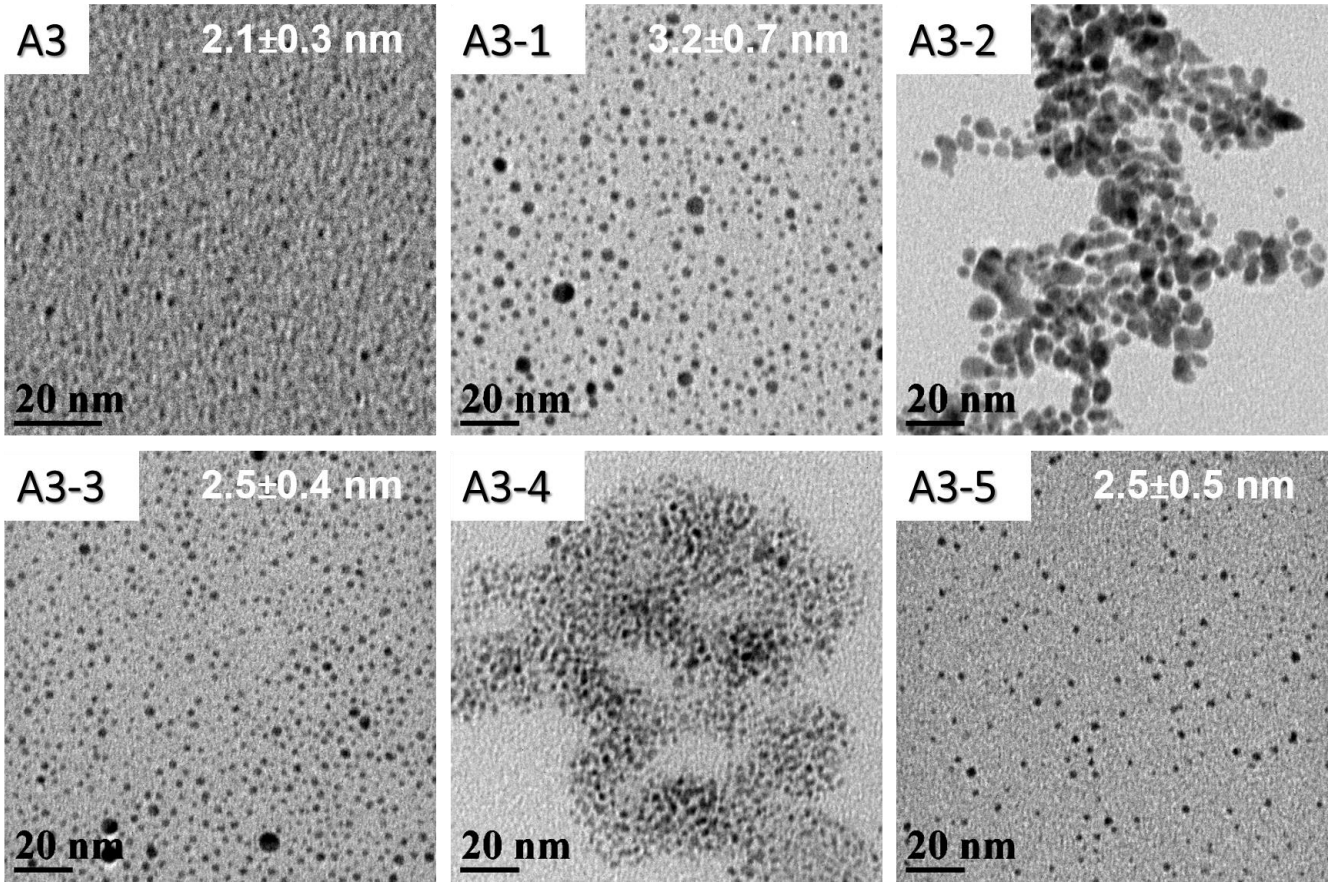

Figure 5. Nguyen *et al.*

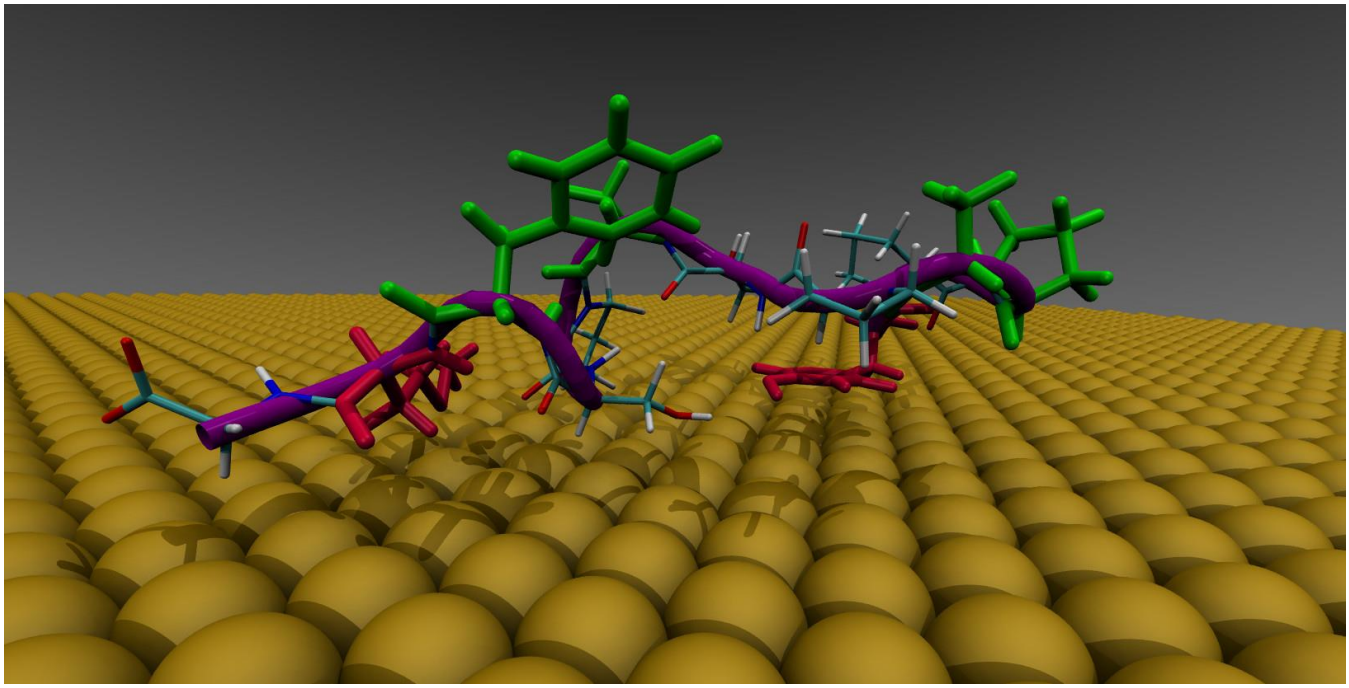

Figure 6. Nguyen *et al.*

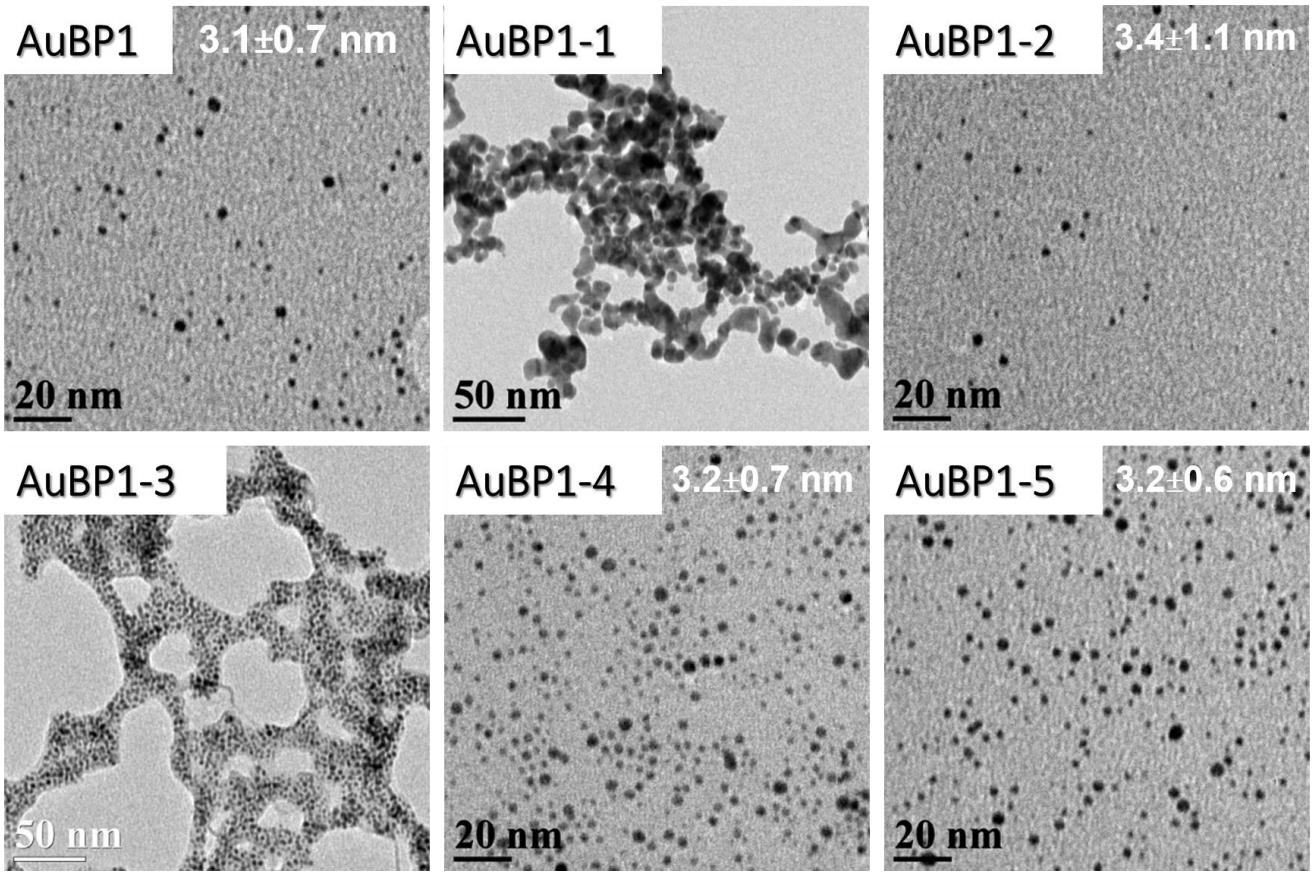

Figure 7. Nguyen *et al.*

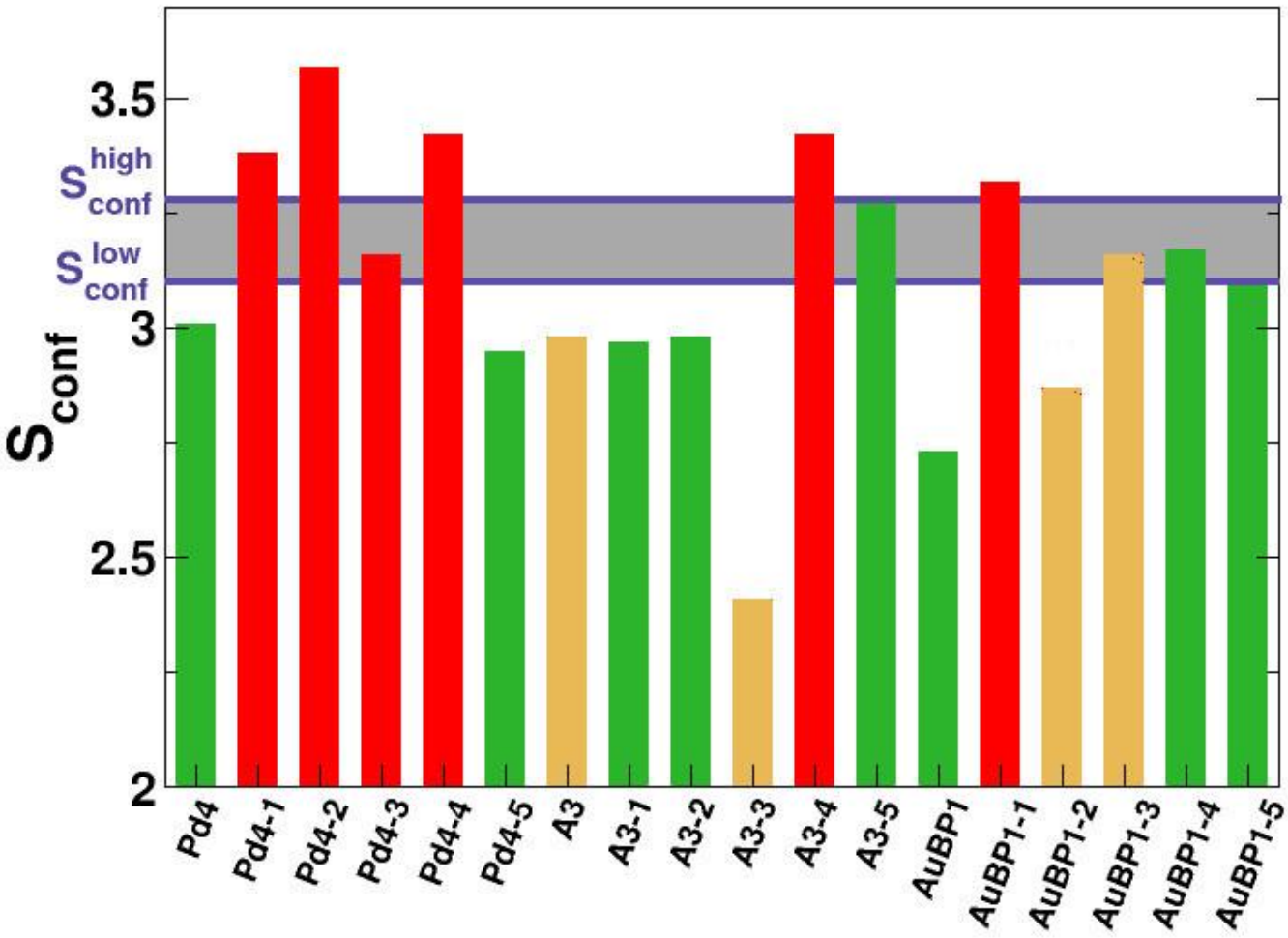

Figure 8. Nguyen *et al.*

ToC Image:

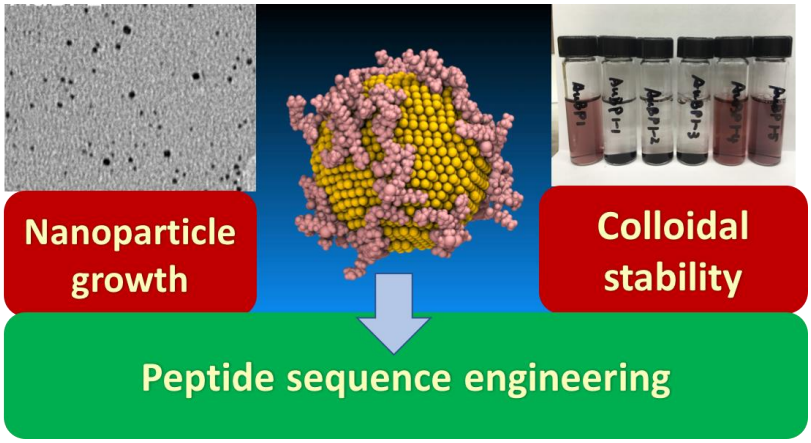
Nanoparticle growth
Colloidal stability
Peptide sequence engineering